

AD A 048621

12

ION PLASMA ELECTRON GUN RESEARCH

W.M. Clark and J.A. Palmer

Hughes Research Laboratories

3011 Malibu Canyon Road

Malibu, CA 90265

December 1977

Contract N00014-77-C-0484

Final Report

For Period 1 June 1977 through 15 November 1977

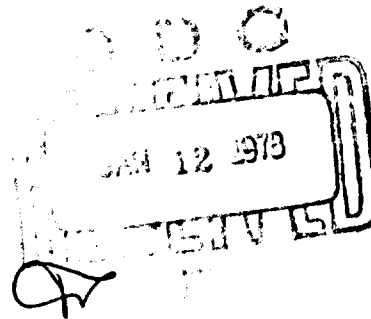
The views and conclusions contained in this document are those of the authors and should not be interpreted as necessarily representing the official policies, either expressed or implied, of the Defense Advanced Research Projects Agency or the U.S. government.

Prepared For

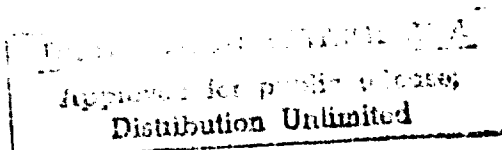
OFFICE OF NAVAL RESEARCH

800 N. Quincy Street

Arlington, VA 22217



DC FILE COPY



UNCLASSIFIED

SECURITY CLASSIFICATION OF THIS PAGE (When Data Entered)

REPORT DOCUMENTATION PAGE		READ INSTRUCTIONS BEFORE COMPLETING FORM
1. REPORT NUMBER	2. GOVT ACCESSION NO.	3. RECIPIENT'S CATALOG NUMBER
4. TITLE (and Subtitle) ION PLASMA ELECTRON GUN RESEARCH,		5. TYPE OF REPORT & PERIOD COVERED Final Report, 1 Jun 77 - 15 Nov 77
6. AUTHOR(s) William M. Clark, Jr. A.J. Palmer		7. PERFORMING ORG. REPORT NUMBER
8. PERFORMING ORGANIZATION NAME AND ADDRESS Hughes Research Laboratories 3011 Malibu Canyon Road Malibu, CA 90265		9. CONTRACT OR GRANT NUMBER(s) N00014-77-C-0484 WARPA Order-1807
10. CONTROLLING OFFICE NAME AND ADDRESS Office of Naval Research 800 N. Quincy Ave. Arlington, VA 22217		11. PROGRAM ELEMENT PROJECT, TASK AREA & WORK UNIT NUMBERS Program Code 7E20 ARPA Order No. 1807 Amendment 24
12. MONITORING AGENCY NAME & ADDRESS (if different from Controlling Office) DARPA 1400 Wilson Blvd. Arlington, VA		13. REPORT DATE 9 Dec 77
14. DISTRIBUTION STATEMENT (for this Report) DEFENSE DOCUMENT A Approved for public release; Distribution Unlimited		15. NUMBER OF PAGES 39 p.
16. DISTRIBUTION STATEMENT (for the abstract entered in Block 20, if different from Report) Approved for public release; distribution unlimited.		15. SECURITY CLASS. (for this report) UNCLASSIFIED
15a. DECLASSIFICATION DOWNGRADING SCHEDULE		
17. SUPPLEMENTARY NOTES The views and conclusions contained in this document are those of the authors and should not be interpreted as necessarily representing the official policies, either expressed or implied, of the Defense Advanced Research Projects Agency or the U.S. government.		
18. KEY WORDS (Continue on reverse side if necessary and identify by block number) e-beam pumped excimer laser, high voltage-high current density		
19. ABSTRACT (Continue on reverse side if necessary and identify by block number) Experiments have been run and a comprehensive theoretical model developed which have enabled a more complete characterization of the ion plasma electron gun. The experiments provided important high current data on the operation of the gun and of the thin-wire discharges. The theoretical model included consideration of fifteen different reactions between helium atoms and ions and electrons and calculated the particle		

172600

and
page
JAN 12 1978
F

UNCLASSIFIED

SECURITY CLASSIFICATION OF THIS PAGE(When Data Entered)

fluxes and the electric potential as a function of position in the high-voltage region. These calculated quantities described accurately the behavior of the gun at a beam voltage of 110 kV and enable a projection of operation of the e-gun at higher voltages, such as 400 keV, with a beam current of 10 A/cm² where the gun will be useful to pump excimer lasers. A qualitative understanding was obtained of the transient behavior of both the e-gun and of the scaling properties of the thin-wire discharges.

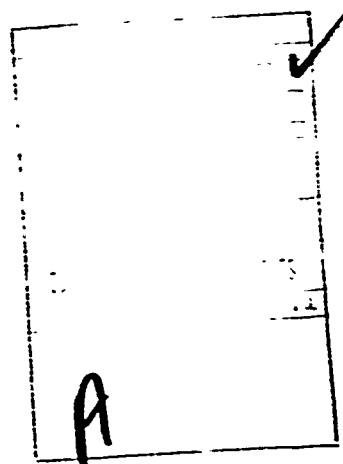
59 cm

UNCLASSIFIED

SECURITY CLASSIFICATION OF THIS PAGE(When Data Entered)

TABLE OF CONTENTS

SECTION		PAGE
	LIST OF ILLUSTRATIONS	4
1	INTRODUCTION	6
2	OPERATING CHARACTERISTICS OF THE ION PLASMA ELECTRON GUN	8
	A. Basic Concept	8
	B. Experimental Results	9
3	THEORETICAL STUDIES	16
	A. Model of the Acceleration Region	16
	B. Model of the Wire Discharge	28
	C. Model of the Transient Behavior of the Gun	31
4	SUMMARY	34
	REFERENCES	36



LIST OF ILLUSTRATIONS

FIGURE		PAGE
1	E-gun schematic	8
2	Photograph and schematic of the thin-wire plasma-discharge chamber with 17 transverse-running wires	11
3	Cathode current and cathode current flux plotted versus total anode wire current at a beam voltage of 110 kV and a helium gas pressure of 20 mTorr	13
4	Anode current and cathode current taken at a beam voltage of 110 kV and a helium gas pressure of 20 mTorr	13
5	Thin-wire discharge test chamber	14
6	Energy dependence of reaction No. 1, symmetric charge exchange	19
7	Energy dependence of reaction No. 2, ion stripping	19
8	Energy dependence for the cross sections for reactions 3 and 4	20
9	Energy dependence for the cross section of reaction 5	20
10	Energy dependence for the cross section of reaction No. 7	21
11	Ionization cross section of helium by electrons from Refs. 20 and 21	21
12	Cross section for reaction 10	22
13	Cross section for reaction No. 13	22
14	Computer program flow chart	23
15	Secondary emission coefficient	24
16	Cathode current versus anode current, theory and experiment	26

FIGURE		PAGE
17	Theoretical calculations of the particle flux and the potential distributions	26
18	Theoretical cathode current-pressure characteristic	27
19	Theoretical I-V characteristic	28
20	Electron orbits in the discharge region	30
21	Transient response: theory	32

SECTION 1

INTRODUCTION

Proof of the concept of the ion-plasma electron gun was accomplished in 1976 on ARPA/ONR contract N00014-72-C-0496. The results showed that this e-gun could be used for pumping repetitively pulsed e-beam-sustained excimer lasers, where it would have compelling advantages over both cold-cathode field-emission and thermionic e-guns. The objective of the present program was to develop a theoretical model for the ion-plasma e-gun that would predict the operating characteristics of the gun at beam voltages useful for pumping excimer lasers. Such a model was developed. Experiments run to corroborate it showed that the model accurately describes the operation of the e-gun at lower beam voltages (up to 150 keV) and that operation of the gun at a beam voltage of 400 kV with a current density of 10 A/cm^2 may be realistically expected.

Although improved results have recently been reported, the development of an efficient, high-average-power, rare-gas monohalide excimer laser system has not yet been fully realized. E-beam-controlled discharge pumping¹ is a promising scheme for obtaining the desired goals for this kind of laser, especially since 1- μsec laser pulses² have recently been attained and since it appears that even longer pulse lengths should be possible at a higher efficiency. Previous studies showed that an e-beam of approximately 400 keV and 10 A/cm^2 is required to pump the laser system. The development of an e-gun to meet these requirements is necessary to the usefulness of these lasers, especially with the added need for repetitively pulsed operation. The ion plasma e-gun, which we describe, has important advantages for pumping this kind of laser and has the potential of attaining the required 400 keV, 10 A/cm^2 beam parameters. The advantages are

- Monoenergetic Beam: The large accelerating voltage for the gun is dc and is not switched. This means there are no low-energy electrons in the beam from the turn-on or turn-off of the accelerating voltage. The energy spread of the beam, caused by atomic mechanisms at the cathode surface, is expected to

be <40 eV.^{3,4} At a beam voltage of 400 keV, this represents an energy spread of $<0.01\%$. Because the output beam is nearly monoenergetic, foil heating will be less and energy will be deposited more uniformly in the laser mixture. This latter characteristic will mean that larger sustainer fields, and hence larger sustainer enhancement, will be possible. With cold-cathode field-emission guns, the nonuniform deposition of energy in the laser mixture (caused by low-energy electrons in the beam) has seriously limited the amount of sustainer energy that can be deposited before instability driven arcs (caused by the non-uniform secondary electron background) curtail laser operation.

- Long Pulse Length: Because there is no plasma closure effect, the gun can operate with longer pulse widths than cold-cathode field-emission guns and without losing current density at the longer pulse lengths. The gun has also operated cw. The attainment of longer pulse lengths means that a larger average laser power output may be obtained for a given repetition frequency.
- Gun Control with Electronics at Ground Potential: The gun is controlled by a thin-wire plasma discharge that is run 1 kV above the ground electrode (anode) voltage of the gun. This simplifies the system requirements for repetitively pulsed operation because only low-voltage switching is required (in contrast to cold-cathode guns) and no power supplies need be floated at high voltage (as with a thermionic gun).
- Scalable: The gun may be scaled simply to pump practical sized lasers.

Section 2 describes the operation of the ion plasma e-gun and presents the experimental results obtained. In Section 3, the theoretical model of the gun is explained and the projected operation of the e-gun at high voltages is given. Section 4 summarizes the results and conclusions of the program.

SECTION 2

OPERATING CHARACTERISTICS OF THE ION PLASMA ELECTRON GUN

A. BASIC CONCEPT

A schematic of the ion plasma e-gun is shown in Figure 1. A low-voltage plasma is struck near the anode that acts as a source of ions. The plasma may be obtained by several means, including a thermionic-diode discharge,⁵ a hollow-cathode discharge, or a thin-wire discharge. A fraction of the ions produced in the discharge are accelerated to the cathode (negative high voltage of as much as 400 kV), where they collide with the electrode surface and produce secondary electrons. These electrons are then accelerated back toward the anode, experiencing few collisions as they pass through the low-pressure gas (the mean free path for 100 kV electrons in 20 mTorr of helium is ≈ 100 m).⁶ This e-beam then passes through the thin foil window and into the laser chamber or the region where the beam is to be used.

4176-2R1

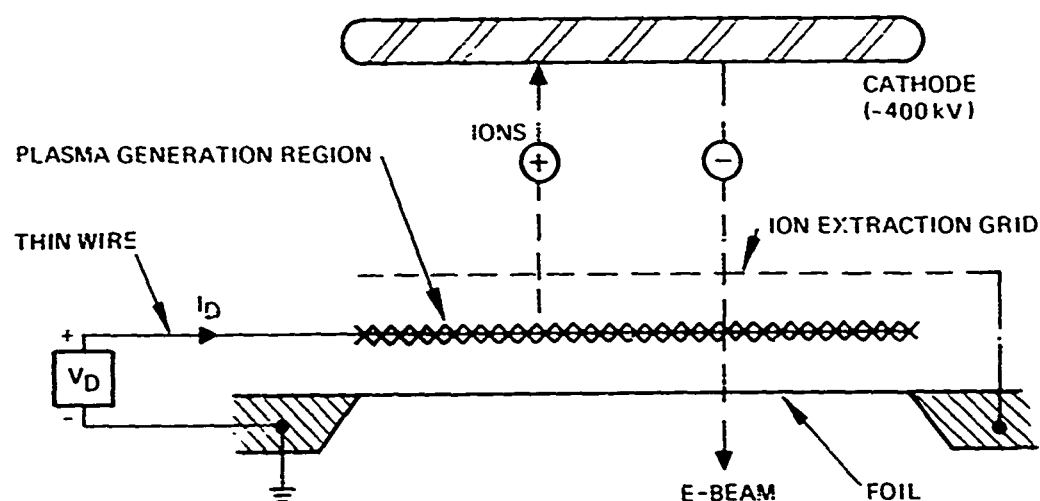


Figure 1. E-gun schematic.

Only the thin-wire discharge operates at a pressure low enough to be compatible with high-voltage operation and can be used with a compact design configuration. The thin-wire discharge, which has been experimentally studied by McClure,⁷ can operate at low pressure because the thin wire permits highly efficient electrostatic trapping of electrons to sustain the discharge. In this discharge, electrons are trapped in the electric field near the thin wire (at a positive voltage of ≈ 400 V) and form helical orbits around the wire. These orbits allow the electrons to attain long path lengths so that ionization of helium atoms can occur (ionization mean free path in 10 mTorr of helium for 400 eV electrons is 70 cm).⁶ This mechanism results in a limited sustaining generation of electrons. In the present experiments, this thin-wire discharge has been operated with pressures as low as 2 mTorr in helium.

An array of thin wires (each wire separately driven) in the ion-plasma e-gun can be distributed across the beam aperture and in the discharge region. Since the depth of the discharge region may be as small as 1 cm, it will not add much to the size of the gun. A hollow-cathode discharge is also an efficient ion source, but, for operation at pressures < 10 mTorr, the ratio of hollow-cathode surface area to extraction area must be increased significantly to obtain meaningful currents. A larger area ratio will increase gun size. Using a thermionic cathode discharge as an ion source allows low-pressure operation, but again size must be significantly increased to accommodate the cathode heaters.

B. EXPERIMENTAL RESULTS

Experiments were run to determine the output current density of the gun as a function of beam voltage, gas pressure, and thin-wire anode current. The data from these experiments was similar to and augmented that obtained previously.⁸ In addition, experiments to characterize the thin-wire discharge mechanisms were performed in a chamber with three-thin-wire discharges. Spatially resolved measurements of the ion production by the thin-wire discharges were also made.

The tests to measure the output current were run on a gun with a 4 cm x 40 cm rectangular e-beam aperture. The high-voltage acceleration region is defined by a flat stainless-steel cathode surface

separated by 4 cm from the ion extraction grid. This grid, which is made of fine stainless-steel wire mesh, has approximately 80% transmission with a wire size of 0.03 mm and a square mesh size of 0.6 mm. The dimensions of the plasma-generation chamber are 4 cm x 4 cm x 40 cm. In this chamber, 17 tungsten wires each 0.3 mm in diameter are placed 2.1 cm apart and run in the transverse direction (4 cm) in the midplane of the discharge chamber. A photograph and a schematic of this scheme are shown in Figure 2. The 0.025-mm-thick (0.001 in.) aluminum foil window is placed on a ribbed aluminum support structure with 80% transmission. For some tests, solid stainless-steel plate was used in place of the foil and support combination.

The high-voltage source for the gun consisted of a dc high-voltage power supply and an energy storage circuit. The energy-storage circuit, which has an effective capacitance of 0.2 μf , has a series isolation resistor (located between the circuit and the gun) with a resistance that was varied between 1 and 10 Ω . The ratings of the components for the circuit elements were picked to allow a beam voltage as high as 200 kV. Because, in operation, these circuit elements regularly failed at voltages above 140 kV, data was taken primarily at beam voltages of 110 to 120 kV. The gun current was controlled with the thin-wire discharges. Each of the 17 wires was driven by its own 0.01- μF capacitor charged to a voltage between 0.8 and 1.4 kV, and with a series ballast resistance of 47 Ω per wire. A single thyratron (type 5C22) was used to switch the voltage across all the wires. The ratio of total current switched to the current in one single wire indicated that each wire carried approximately the same current.

The total cathode current, which includes both the incident ion current and the secondary emission electron current, was measured with a Pearson model 110 current transformer placed around the wire leading to the cathode. At a given gas pressure, the total cathode current drawn (for a given thin-wire current) varied approximately as $V^{3/2}$, suggesting a Child's law type of behavior. As pressure increased, anode current, cathode current, and the ratio of cathode current to anode current all increased. The theoretical model (discussed in Section 3) predicts functional relationships of this type.

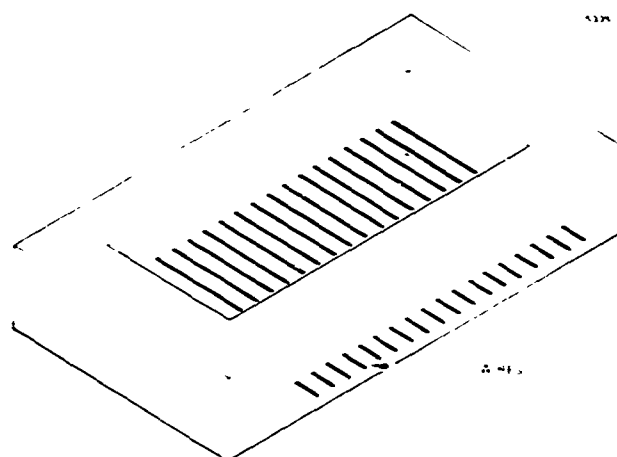
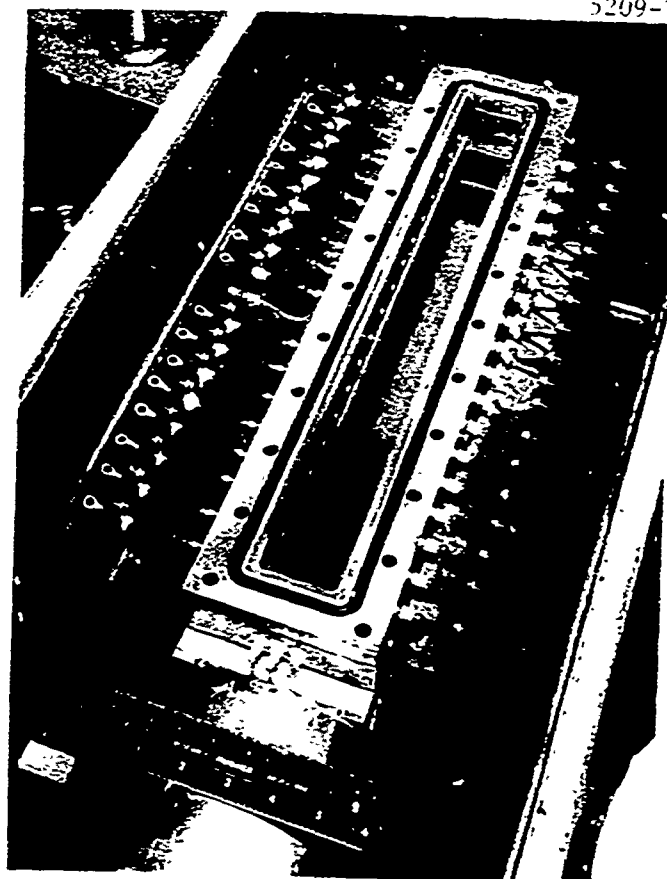


Figure 2. Photograph and schematic representation of the thin-wire plasma discharge chamber with 17 transverse-running wires.

At a beam voltage of 110 kV, the cathode current and the cathode current flux (total cathode current divided by cathode area) are shown plotted as a function of total anode current in Figure 3. Data from earlier experiments with a different thin wire configuration and at longer pulse widths⁸ is included. The plot shows that a nearly linear relationship holds for over four decades of variation in cathode current and anode current including both long-pulse (150 msec) and short-pulse (5 μ sec) operation. The higher current values actually fall beyond a knee in the curve because there is a space-charge constraint on the maximum ion current that can be extracted from the plasma-generation region. This is discussed below. The theoretical model combined with this data shows that, even with the 5- μ sec FWHM current pulse, the gun operates cw insofar as the plasma phenomena are concerned. The maximum pulsed cathode current flux obtained was 2 A/cm^2 (320 A total) at a total anode wire current of 300 A. Figure 4 shows an oscillogram of the current waveforms for the total anode wire current and the total cathode current. Although the anode current pulse is only 2 μ sec FWHM, the cathode current pulse is longer (5 μ sec FWHM) because the fall time is long. The long fall time, which has been observed with other guns of this kind,⁵ is due to the transit time for ions to escape from the plasma discharge region once the thin-wire voltage has dropped to zero. (This is discussed further in Section 3).

Thin-wire discharge studies were performed with a discharge test chamber that has three wires spaced 2.1 cm apart and the same transverse dimensions (4 cm x 4 cm) as the 17-wire assembly described above. The dimensions of the ion-extraction grid for this device are 4 cm x 9 cm, and the grid is made of the same materials as is the 17-wire assembly. A Faraday cup ion collector is located less than 1 cm beyond the ion-extraction grid. The Faraday cup has a 0.6-cm-diameter aperture and can be moved along the 9-cm dimension of the grid aperture. The Faraday cup was biased at -25 V with respect to the ion-extraction grid, and the suppressor grid at the entrance of the cup was biased at -50 V relative to the extraction grid. This arrangement is shown schematically in Figure 5.

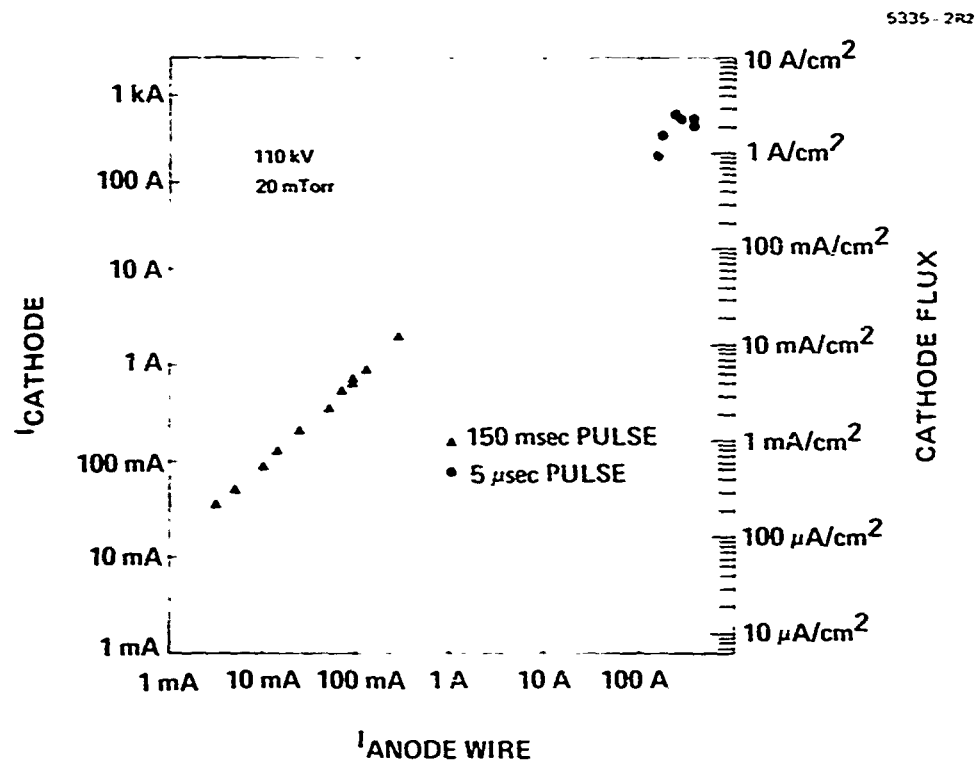


Figure 3. Cathode current and cathode current flux plotted versus total anode wire current at a beam voltage of 110 kV and a helium gas pressure of 20 mTorr.

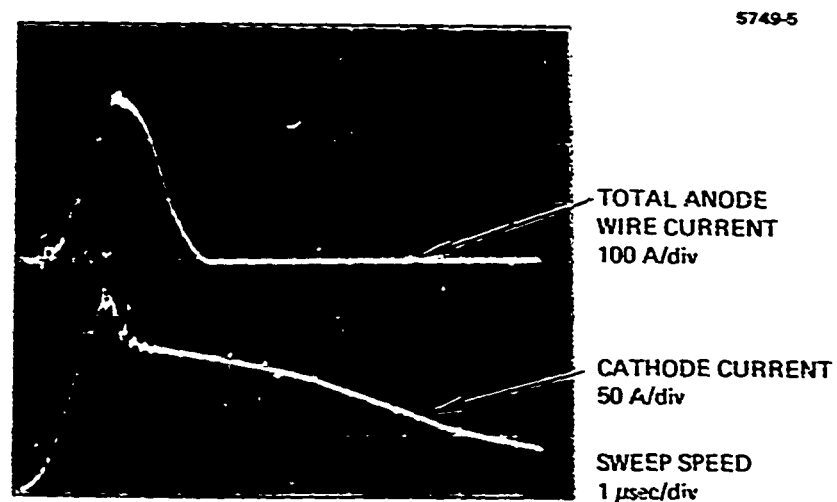


Figure 4. Anode current and cathode current taken at a beam voltage of 110 kV and a helium gas pressure of 20 mTorr.

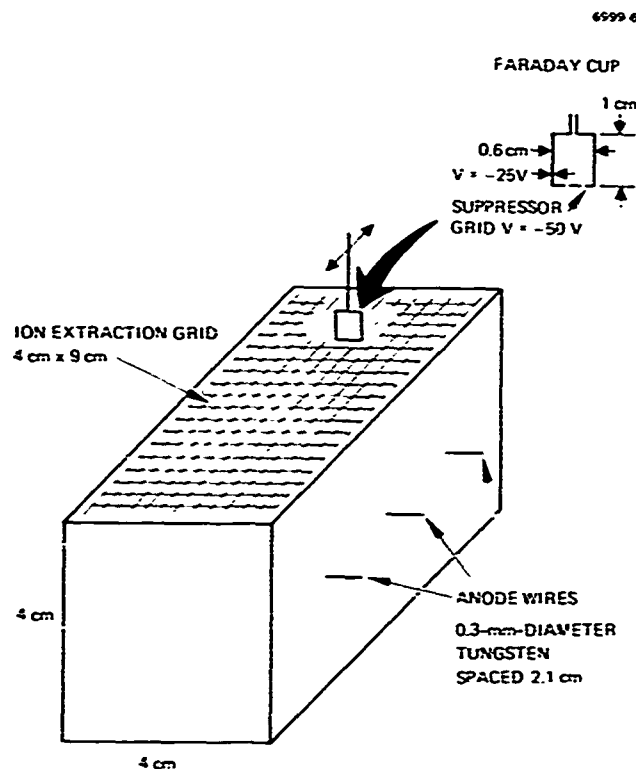


Figure 5.
Thin-wire discharge test
chamber.

This thin-wire discharge chamber facilitated studying the discharge mechanisms. Wire voltages and currents were monitored as the gas pressure was varied. Two different wire driving mechanisms were used: the charged-capacitor arrangement described above and a hard tube Velonex type 350 pulser with both a 200 Ω and a 50 Ω output transformer, each capable of 1 to 10 μ sec pulse lengths. In each case, the spatial uniformity of the ions produced in the discharge and extracted through the grid was measured with the Faraday cup collector.

With the three wires driven in parallel by the pulser, current-voltage (I-V) data was taken as a function of gas pressure. Two different operating regimes for the discharge were observed. These regimes were characterized by quite different observed discharge voltages for identical pressure and current conditions. At wire currents of approximately 10 A or less (≈ 30 A total anode current), the discharge voltage was high (≈ 800 to 950 V, depending on gas pressure). As the pulser amplitude control was turned up and the current increased, the

discharge would first run in the same mode as above (i.e., discharge voltage ≈ 800 to 900 V), but then the voltage would suddenly drop to ≈ 250 V or less with the current remaining the same. The point where this discharge voltage collapsed was neither predictable nor repeatable. We believe that this voltage collapse represents a collapse of the glow discharge into a filamentary type of discharge. No change in the spatial uniformity of the ion current collected by the Faraday cup was observed when the voltage decreased. When operating in the high-voltage regime (lower currents), the discharge followed the I-V and pressure (P) characteristics of a glow discharge fairly well (i.e., I/P^2 was approximately constant for a given discharge voltage). This is discussed in Section 3.

Spatially resolved measurements of the ion current collected by the Faraday cup were taken at various currents and gas pressures and with both kinds of excitation. The results did not differ significantly by case. The spatial uniformity of the ion current was very good, $\pm 5\%$ within the center of the aperture with a smooth fall off in current density at positions within 1 cm of the walls of the discharge region.

SECTION 3

THEORETICAL STUDIES

This section discusses the development of a model of the ion plasma e-gun. Three facets of gun behavior were studied:

- The steady-state behavior of the high-voltage accelerating region
- The steady-state behavior of the low-voltage wire discharge ion source
- The transient behavior of the gun.

A. MODEL OF THE ACCELERATING REGION

The accelerating region of the gun is the gap between the grounded ion-extraction grid and the cathode, which is held at a negative high voltage. An essentially one-dimensional flow of helium ions, neutrals, and electrons traverses this gap. The flow of these species is controlled by the space-charge field, by collisions, and by secondary emission at the cathode. Because the flow is one dimensional and the various collision cross sections and secondary emission coefficients are fairly well known functions of energy, the accelerating region may be analyzed quantitatively via numerical computations. The computer program used for the analysis is similar to one used previously by McClure⁹ for modeling the cathode region of high-voltage glow discharges in deuterium. As in that case, our model assumes that the electric field is the sole factor affecting the energy of a particle from the time it is created until it is destroyed (i.e., changed to another species). This is justified by the fact that the energy losses suffered by both ions and electrons from ionizing collisions are negligible compared to the energy gain from the electric field in one ionization mean-free path. Also, the secondary effects produced by electrons released in gaseous collisions are ignored. With the high cathode fall potentials to be considered, the probability that an electron released anywhere within the accelerating region will undergo an ionizing collision before passing through the acceleration region is only a few percent. Hence the ion production introduced by secondary electrons produced in the gas is negligible.

The model predicts fluxes of four particle species as a function of position in the accelerating gap for specified values of the accelerating voltage, gap distance, helium pressure, and ion current at the extraction grid. The four species are electrons, singly and doubly charged helium ions, and fast helium atomic neutrals. Molecular species have negligible concentrations for the pressures considered.

The collisional processes included in the model are listed in Table 1, and the cross sections for these processes are presented as a function of energy (in the energy range of interest) in Figures 6 through 13.

The particle fluxes and space-charge field profile across the gap are computed self-consistently. A flow chart for the computer program that performs this calculation is presented in Figure 14. Three basic equations were used in the computer program. The first is Poisson's equation (integral form):

$$E(x) - E(0) = 4\pi e \int_0^x \int_0^{\epsilon_{\max}} \frac{1}{(2\epsilon)^{1/2}} \left[\phi^+(\epsilon, x) + \phi^{++}(\epsilon, x) \right] d\epsilon dx, \quad (1)$$

where $E(x)$ is the electric field at a distance x from the accelerating grid, $\phi^+(\epsilon, x)$ and $\phi^{++}(\epsilon, x)$ are the singly and doubly charged helium ion fluxes per unit energy and distance interval, and ϵ_{\max} is the maximum kinetic energy ($=eV(x)$ or $2 eV(x)$) possible for ions at position x . The second is the continuity equation for the particle fluxes:

$$\frac{\partial \phi_i}{\partial x} + \frac{q_i}{m_i} E(x) \frac{\partial \phi_i}{\partial \epsilon} = \left[N \sum_{j=1} \sigma_{ji} \phi_j - \sigma_i \phi_i \right], \quad (2)$$

where $i = k, 2, 3, 4$ denotes particles He, He^+ , He^{++} , and e^- , respectively; N is the ambient helium concentration; σ_{ij} is the total cross section for converting species j to species i ; and ϕ_i is the net destructive cross section for species i on the ambient gas. The third is the

Table 1. Collisional Processes Included in the Model

Reactions Considered	Comments
<u>Fast He⁺ destruction</u>	
$\text{He}_f^+ + \text{He} \rightarrow \text{He}_f + \text{He}^+$,	Figure 6
$\text{He}_f^+ + \text{He} \rightarrow \text{He}_f^+ + \text{He} + e$	Figure 7
<u>Fast He⁺⁺ destruction</u>	
$\text{He}_f^{++} + \text{He} \rightarrow \text{He}_f + \text{He}^{++}$	Figure 8
$\text{He}_f^{++} + \text{He} \rightarrow \text{He}_f^+ + \text{He}^+$	Figure 8
<u>Fast He destruction</u>	
$\text{He}_f + \text{He} \rightarrow \text{He}_f^+ + \text{He} + e$	Figure 9
$\text{He}_f + \text{He} \rightarrow \text{He}_f^{++} + \text{He} + e + e$	Figure 12
<u>Slow He⁺ production</u>	
$\text{He}_f^+ + \text{He} \rightarrow \text{He}_s^+ + \text{He}_f^+ + e$	Figure 10
$\text{He}_f + \text{He} \rightarrow \text{He}_s^+ + \text{He}_f + e$	Neglect (Ref. 16)
$e + \text{He} \rightarrow \text{He}_s^+ + e + e$	Figure 11
$\text{He}_f^{++} + \text{He} \rightarrow \text{He}_s^+ + \text{He}_f^{++} + e$	Figure 12
<u>Slow He⁺⁺ production</u>	
$\text{He}_f^+ + \text{He} \rightarrow \text{He}_s^{++} + \text{He}_f^+ + e + e$	Neglect (Ref. 15)
$\text{He}_f + \text{He} \rightarrow \text{He}_s^{++} + \text{He}_f + e + e$	Neglect (Ref. 17)
$e + \text{He} \rightarrow \text{He}_s^{++} + e + e + e$	Figure 13
$\text{He}_f^{++} + \text{He} \rightarrow \text{He}_s^{++} + \text{He}_f^{++} + e + e$	Neglect (Refs. 16, 18)
$\text{He}^+ + e \rightarrow \text{He}^{++} + e + e$	Neglect (Refs. 19, 20)

6008

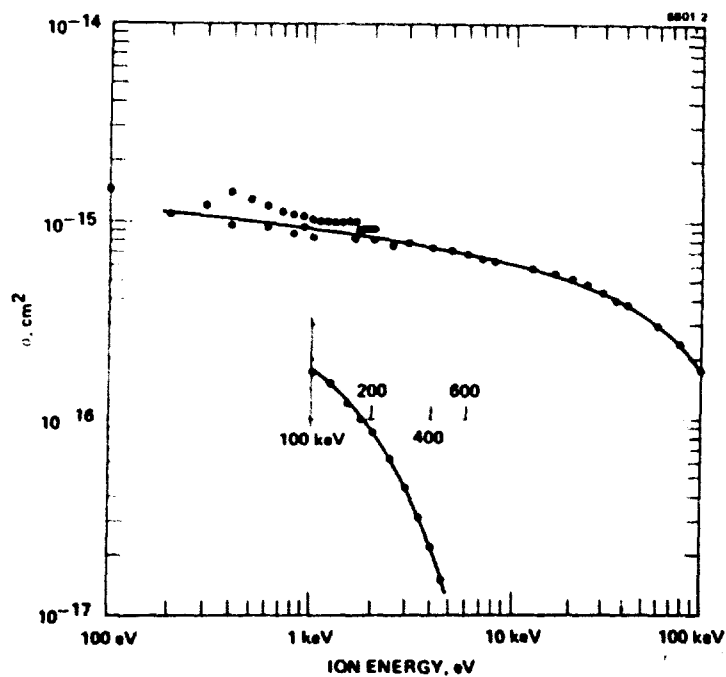


Figure 6.
Energy dependence of
reaction No. 1, symmetric
charge exchange, $\text{He}_f^+ + \text{He} \rightarrow \text{He}_f + \text{He}^+$
slow, as given
by References 12, 13, and
14.

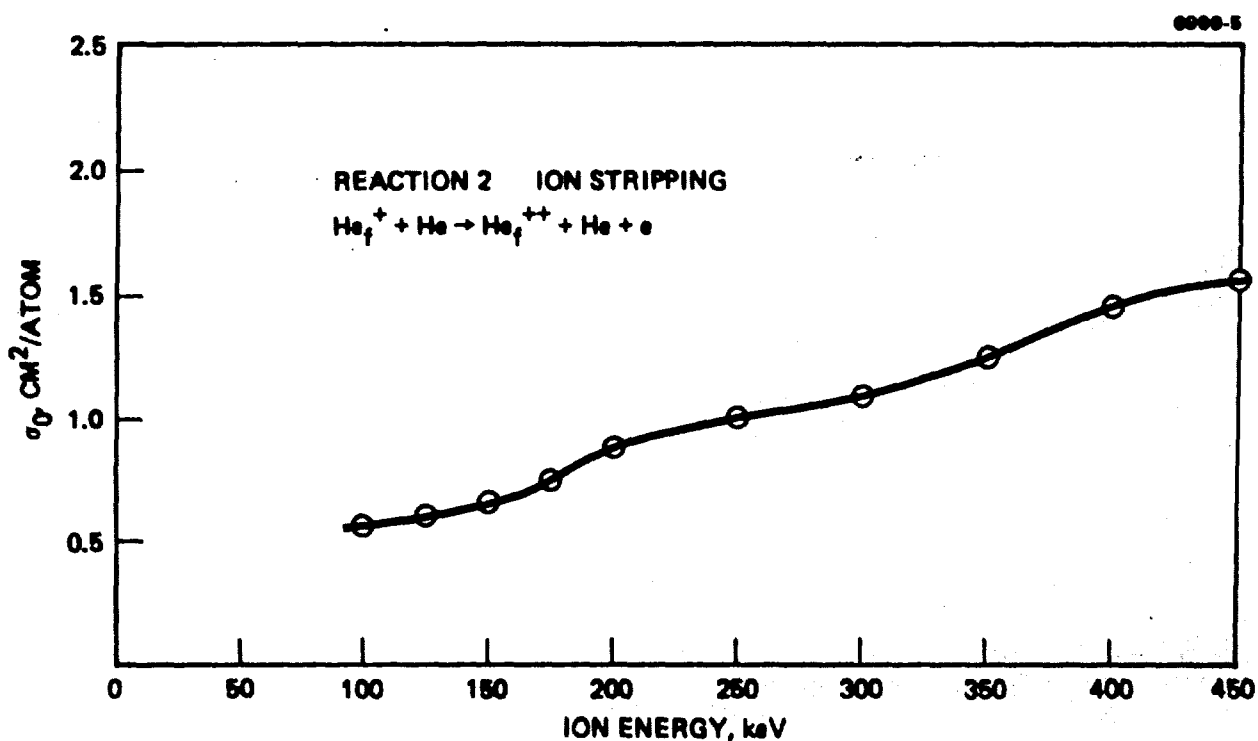


Figure 7. Energy dependence of reaction No. 2, ion stripping, $\text{He}_f^+ + \text{He} \rightarrow \text{He}_f^{++} + \text{He} + e$, from Ref. 12.

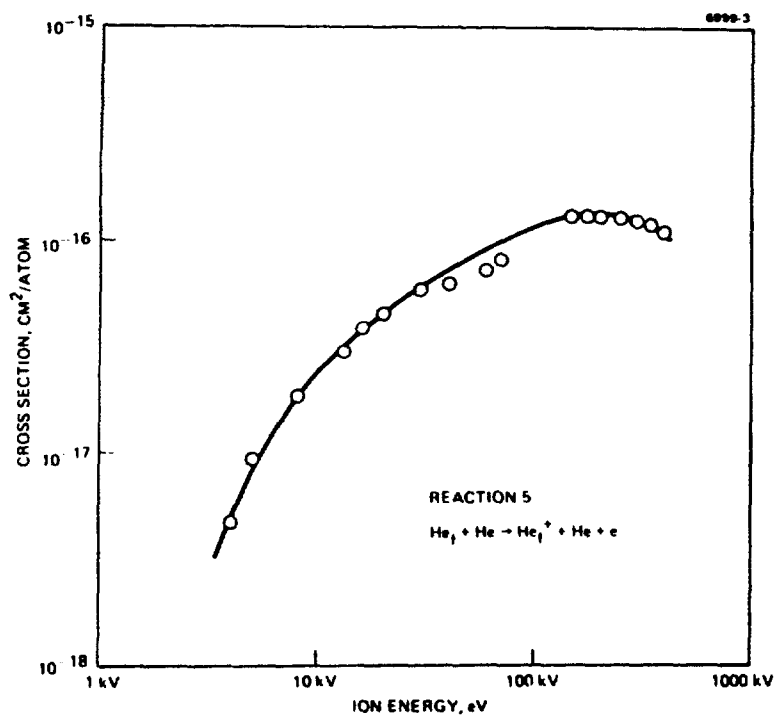
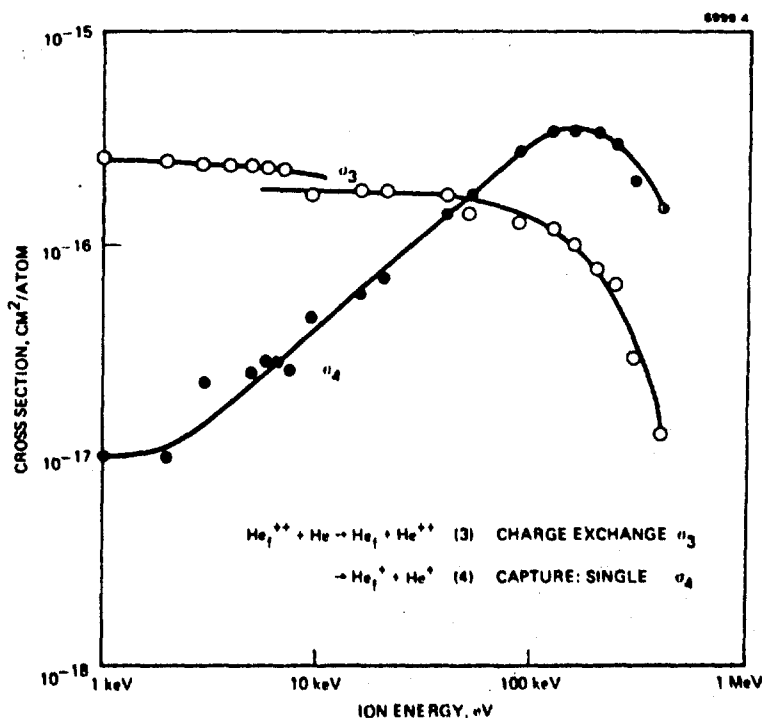


Figure 8.
Energy dependence for the
cross section for reactions
3 and 4. $\text{He}_f^{++} + \text{He} \rightarrow \text{He}_f$
+ $\text{He}^{++} \rightarrow \text{He}_f^+ + \text{He}^+$ from
References 5, 16, and 17.

Figure 9.
Energy dependence for
the cross section of
reaction 5, $\text{He}_f + \text{He} \rightarrow$
 $\text{He} + e$ from References
12 and 18.



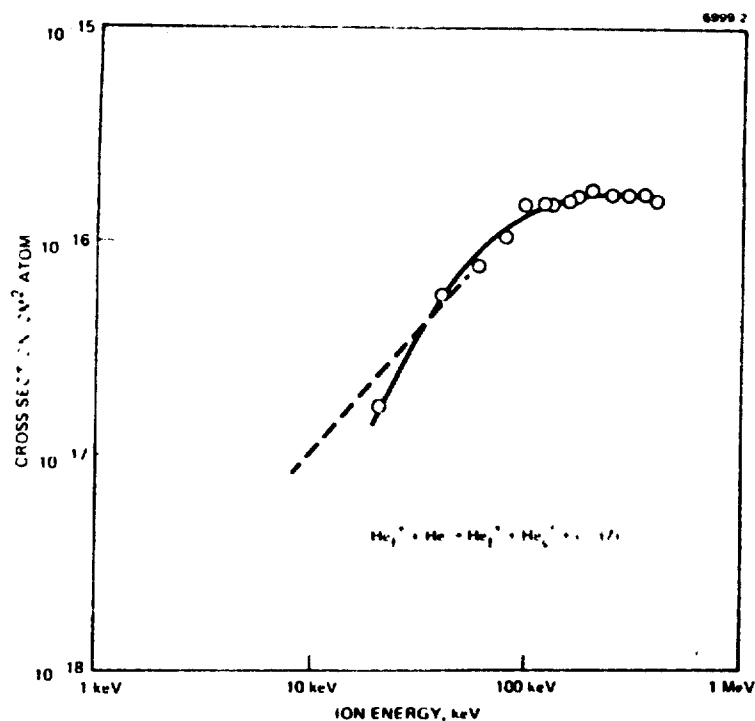


Figure 10.
Energy dependence for
the cross section of
reaction No. 7 $\text{He}_f^+ + \text{He}$
 $\rightarrow \text{He}_f^+ + \text{He}_f^+ + e$ taken
from References 12, 18,
and 19.

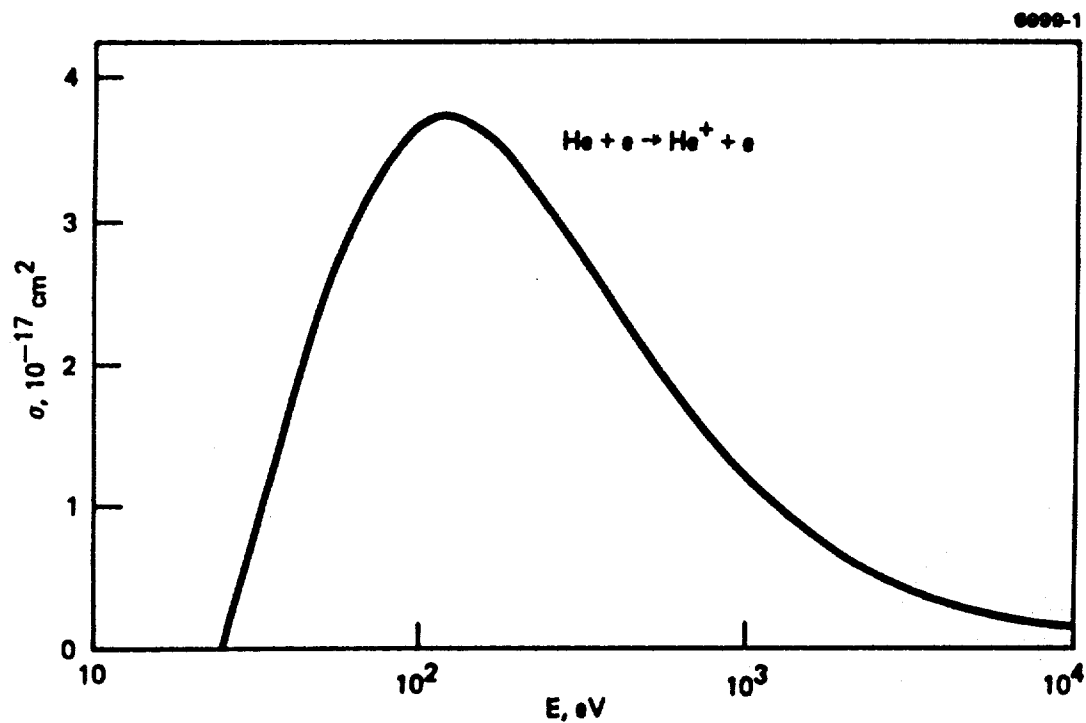


Figure 11. Ionization cross section of helium by electrons from
Refs. 20 and 21.

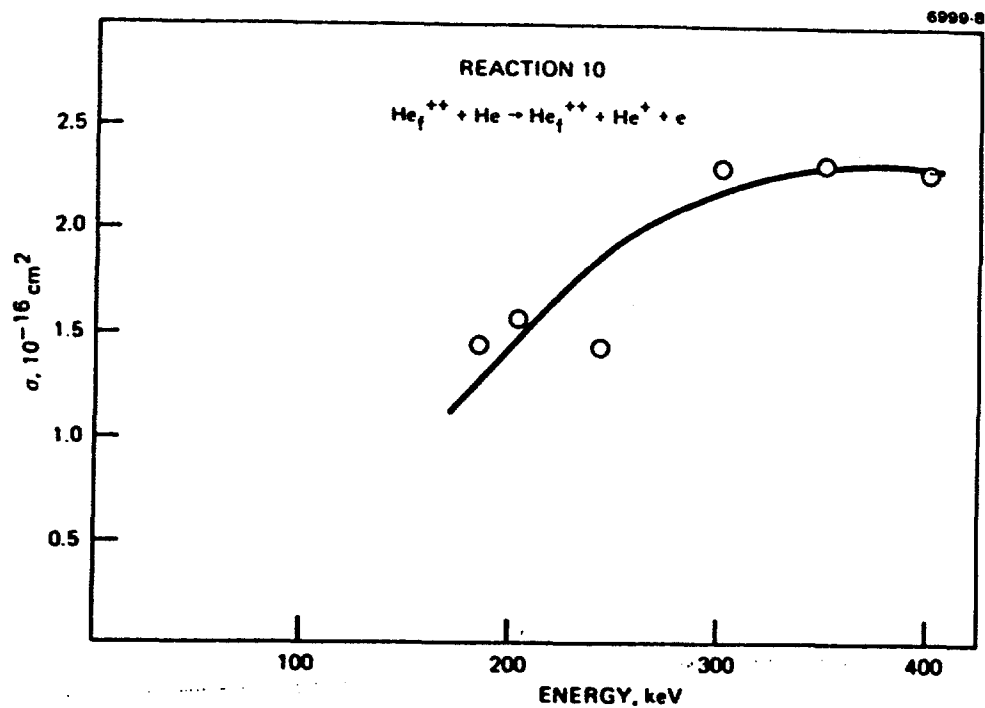


Figure 12. Cross section for reaction 10, $\text{He}_f^{++} + \text{He} \rightarrow \text{He}_f^{++} + \text{He}^+ + e$ from Reference 22.

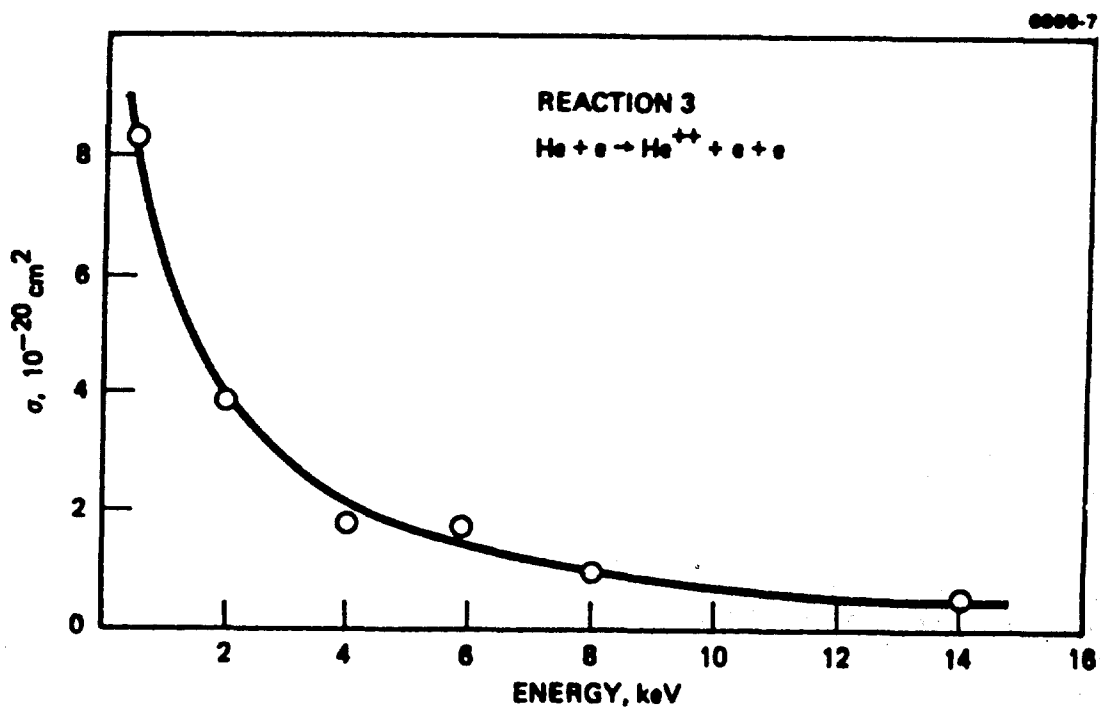


Figure 13. Cross section for reaction No. 13, $\text{He} + e \rightarrow \text{He}^{++} + e + e$ from Ref. 23.

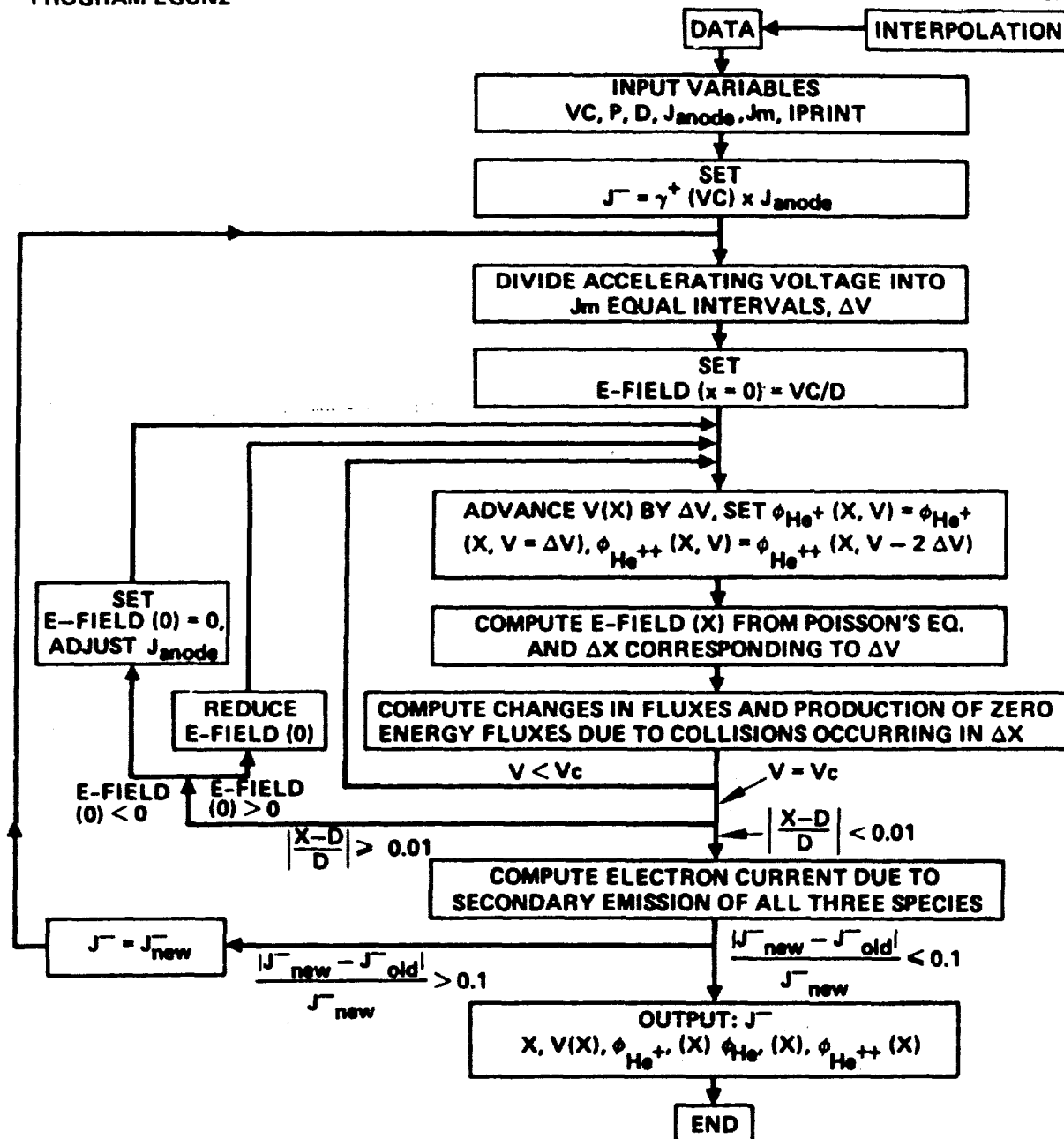


Figure 14. Computer program flow chart.

cathode secondary emission equation:

$$\phi_4(x = d) = \int_0^{V_c} \sum_{i=1}^3 \gamma_i(\varepsilon) \phi_i(\varepsilon, d) d\varepsilon, \quad (3)$$

where d is the gap distance, and the $\gamma_i(\varepsilon)$ are the secondary emission coefficients for electrons due to species i .

There are two basic iterative loops in the computer program displayed in Figure 15. One iteration procedure is performed on the cathode electron current. First, the current is calculated as the product of the secondary emission coefficient (for singly charged ions at the full cathode potential) and the input value of the wire discharge ion current, J_{anode} . Then the cathode electron current is recomputed using the flux of all three species computed by the program. The recomputed value is used in the program and corrected by the new computed particle fluxes until the discrepancy between old and new values of the current is less than 1%.

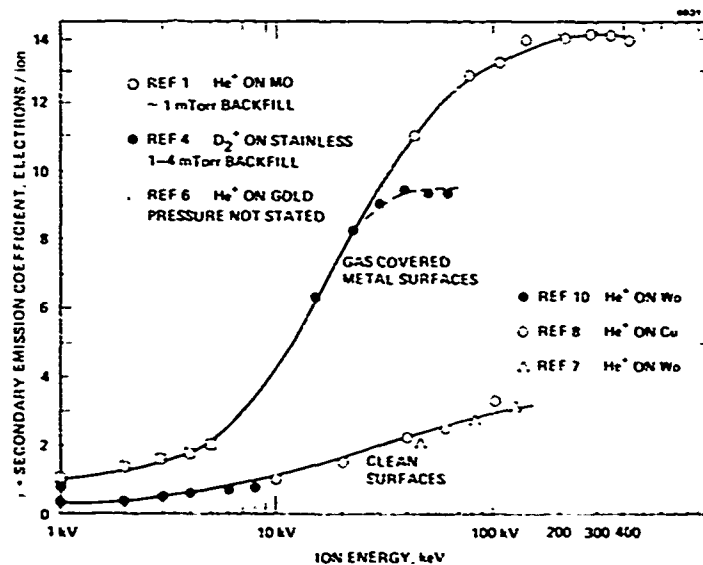


Figure 15. Secondary emission coefficient.

An interaction calculation is also performed on the effective ion current entering the accelerating region and on the corresponding electric field in the gap region. If the wire discharge ion current is small compared with the space-charge-limited ion current in the accelerating gap, then the field will be constant throughout the gap ($E = V_c/D$), and the input wire discharge ion current density, J_{anode} , is used in Eqs. 1 and 2. However, if the ion current is comparable to or greater than the space charge limit, then the field at the extraction grid will be less than V_c/D , becoming negative as J_{anode} exceeds the space charge limit. This means that a virtual anode exists at some negligibly small distance into the accelerating region from the ion-extraction grid. In the program, Poisson's equation is used to compute the electric potential at each position in the accelerating region. At a potential equal to the applied voltage on the accelerating gap, the computed distance is compared with the given gap distance, D . In general, the computed value of distance will be smaller because too large a value for the field at the ion-extraction grid will have been assumed. This boundary value for the field (i.e., potential at the grid) is then reduced until either the computed gap distance falls within 1% of the given value or until the boundary value for the field at the-grid becomes negative (i.e., repels ions). If the latter case occurs, it means that a portion of the wire discharge ion current is being returned by the virtual anode. The program then sets the grid boundary value for the field equal to zero and adjusts the ion current density in the accelerating region downwards until the computed gap distance falls within 1% of the given value. The value of the ion current for which this occurs is the correct space-charge-limited ion current for the conditions inputted.

The results of the ion-plasma e-gun accelerating region predicted by the model are presented in Figures 16 through 18. Figure 16 shows the theoretical e-beam current versus wire discharge ion current at 110 kV and 20 mTorr compared with experimental measurements as presented in Figure 3. Agreement between the model and the observed results is good. The space-charge-limited current regime is clearly shown by the theoretical curve as the "saturation" of the cathode current with

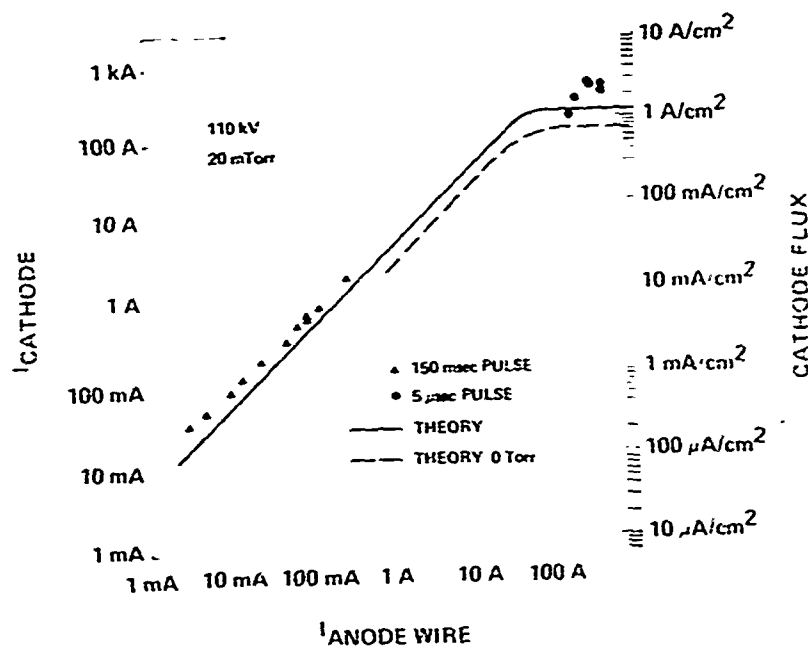


Figure 16. Cathode current versus anode current, theory and experiment.

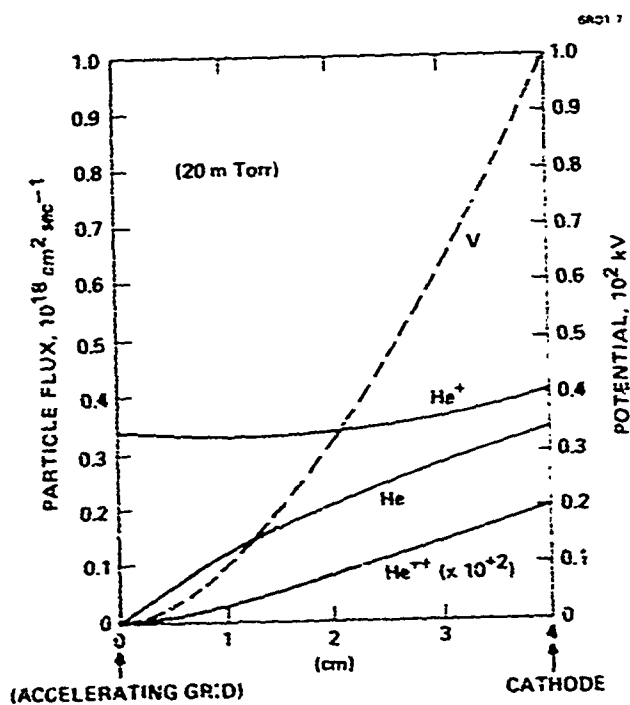


Figure 17. Theoretical calculations of the particle flux and the potential distributions versus position in the accelerating region.

increasing anode current. The theoretical results also reveal that there is a 20% increase in gun current over what would occur in a vacuum accelerating region. This is caused by the added secondary emission by fast helium neutrals, which are generated by charge-transfer collisions within the accelerating region.⁸

The effect of charge-transfer collisions is shown even more clearly in the computed particle flux profiles at positions within the accelerating gap. Figure 17 shows that the flux of helium neutrals generated by charge exchange actually becomes comparable to that of the singly charged ions at the cathode surface. This plot also shows that the flux of doubly charged ions is negligible.

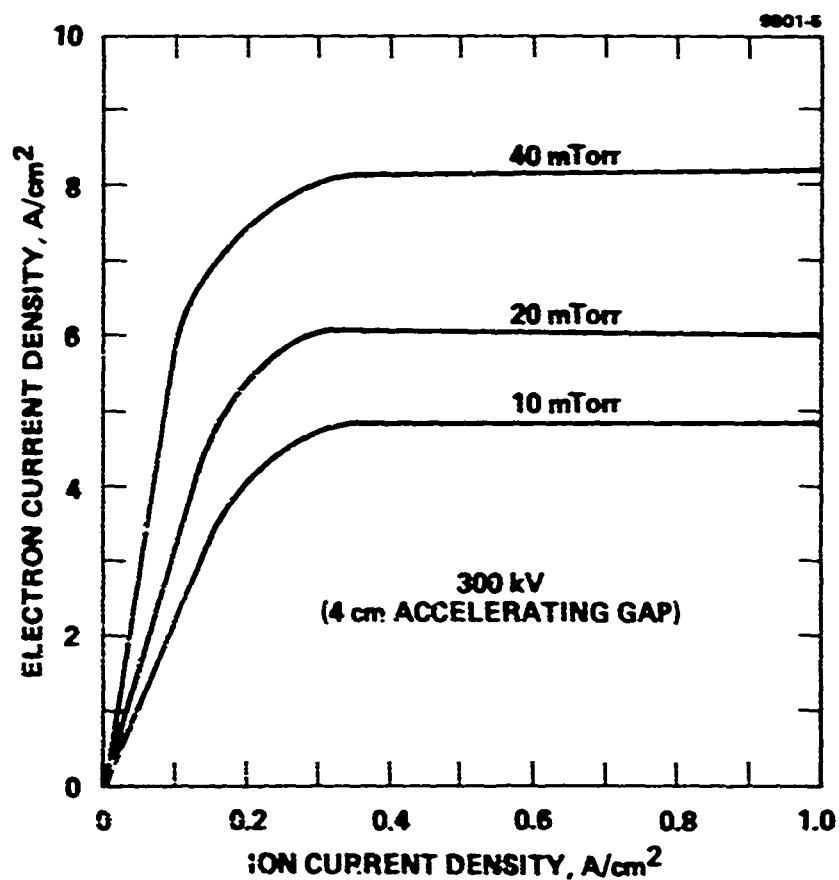


Figure 18. Theoretical cathode current-pressure characteristic.

Figures 18 and 19 present the variation of electron current with anode current, pressure, and beam voltage. Figure 18 shows that currents below the space-charge limit are equal for different voltages. This is because the secondary emission coefficient does not change appreciably in the voltage range shown.

B. MODEL OF THE WIRE DISCHARGE

The wire discharge presents some difficulties for modeling, primarily because it appears to be necessary to include at least two and possibly three dimensions in the characterization of the electron orbitals about the wire.¹⁰ The development of a multidimensional model of the low-voltage discharge would take us far beyond the scope of the present program.

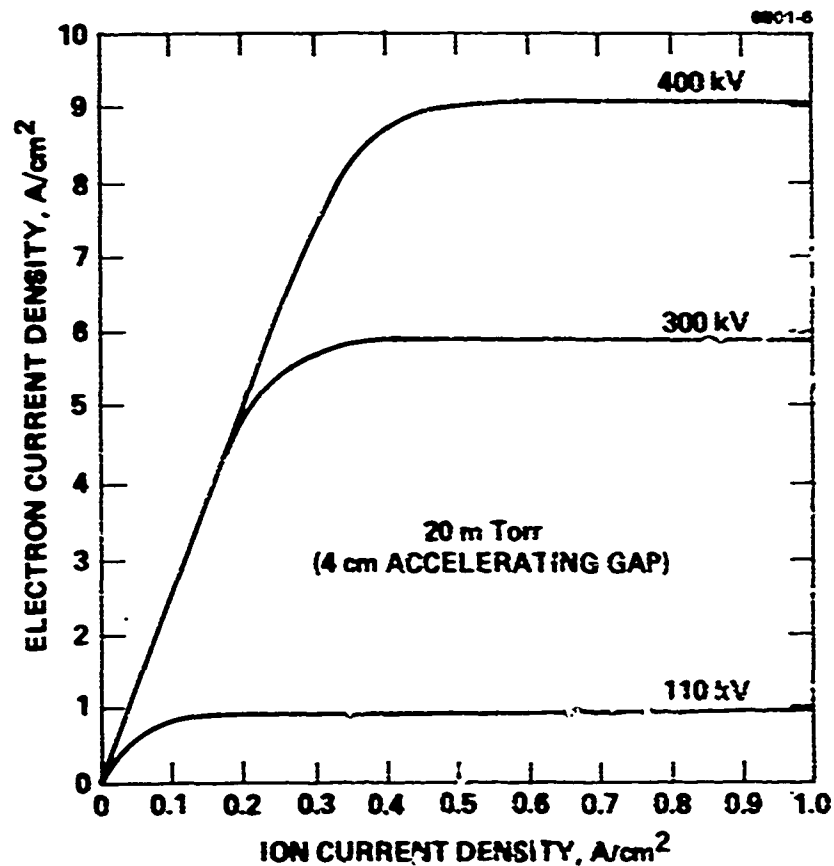


Figure 19. Theoretical I-V characteristic.

There are some physical justifications for a one-dimensional model of the wire discharge. As in the accelerating region, the I-V characteristic of the low-voltage discharge is controlled mainly by the space charge of the positive ions. Unlike the electrons, the ions travel along essentially one-dimensional radial paths to the cathode walls of the discharge (see Figure 20). Also, a low field region that exists near the anode wire of the discharge is analogous to the negative glow of a conventional discharge (which contains most of the electron space charge). It is reasonable to assume that the radial extent of this region, like the electron orbitals themselves, will be comparable to the radial dimension of the discharge because of the large electron mean free path. Since the spacing between adjacent wires in a plasma anode e-gun is also comparable to the radial dimension of the discharge region, there will likely be some overlap of the negative glow surrounding each wire. In this case, the ions will travel along rectilinear one-dimensional paths, as in the case of plane electrodes. The only essential difference between this case and the cathode fall region of a conventional plane electrode discharge is the spiraling orbits of the electrons around the anode wires. We assume that, as in a plane electrode discharge, the electrons do not contribute significantly to the space charge in the cathode fall region but only determine, by their ionization avalanche, the effective location of the negative glow boundary. In particular, we assume that the field increases linearly with distance from the "negative glow boundary" to the cathode as in the plane electrode case.¹¹ The ionization by the electrons can then be simply characterized with a hypothetical ionization cross section large enough to account for the effective trapping of the electrons in spiraling paths about the wires (the large ionization cross section is also used to describe hollow-cathode discharges in a glow discharge model). This will allow Von Engel's model¹¹ of the cathode fall to be applied directly to the wire discharge with the only change being the use of an artificially large electron collisional ionization cross section (determined from experiment).

The mean free path of the ions in the wire discharge is long in comparison with the radial dimension of the discharge. Thus, they will be in free fall from the negative glow to the cathode. Under this condition,

Von Engel's model of the discharge gives the current density as

$$j/p^2 = 2^{-1/2} \pi^{-1} \frac{v^{3/2}}{(Pd)^2} \frac{1 + \gamma_i}{1 - G} \quad (4)$$

with

$$Pd = \frac{1}{\bar{s}/P[1 - \sqrt{Ve/Vc}]} \ln \left(\frac{1}{s_g \gamma_p \gamma_p b V_c} \right), \quad (5)$$

where P is the pressure, d is the effective distance to the negative glow from the cathode, V_c is the cathode fall (discharge voltage in our case), \bar{s} is the effective ionization rate (taking trapping into account), and the constants γ_i , G , Ve , fg , γ_p , γ_p , and s are constants that depend primarily upon the kind of gas and are independent (as a first approximation) of voltage and pressure. The produce Pd given by Eq. 5, is usually assumed to be dependent only on V and independent of P ; since s has a first-order linear dependence on p so s/P is independent of P .

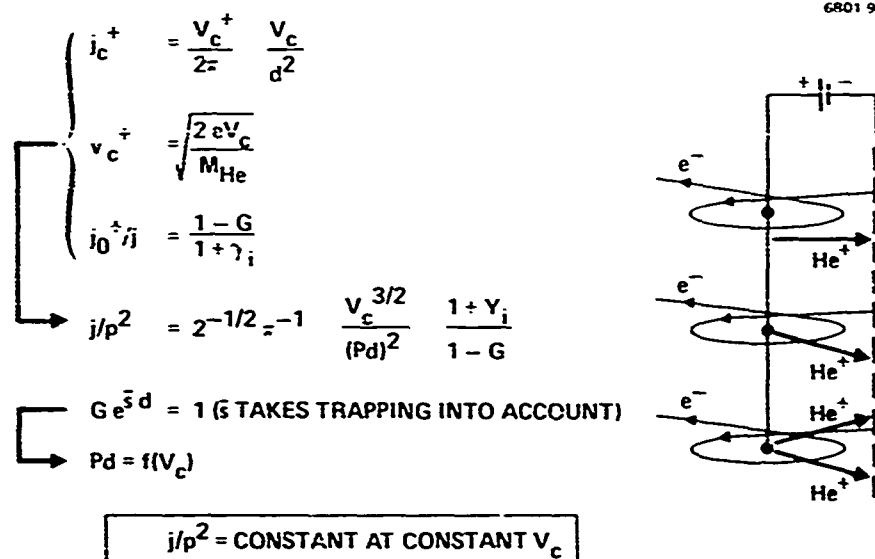


Figure 20. Electron orbits in the discharge region.

Von Engel's model adequately describes the qualitative behavior of the wire discharge and may be made quantitative by normalizing to one experimental data point to fix the value of \bar{s} . Even before such normalization, the model predicts the similarity principle of a constant J/P^2 for a constant voltage for a uniform glow mode of operation (even though the ions are in free fall). This kind of scaling is observed at wire currents ≤ 10 A, but at higher currents the discharge sometimes collapses into filaments.

C. MODEL OF THE TRANSIENT BEHAVIOR OF THE GUN

The primary objective of the theoretical study of the gun's transient behavior is to arrive at an explanation and a method of controlling the relatively long fall time observed for the beam current when the ion current turns off in a much shorter time (see Figure 4).

A qualitative understanding of the physics is all that is required in this case, and the solution can be realized with the aid of Figure 21. The figure depicts the space charge and potential profile in the wire discharge steady-state operation and immediately after the wire anode external power supply circuit is opened. During steady-state operation, some of the positive ions are in free fall between the field-free negative glow region and the accelerating grid, and thus traverse this region with an average velocity

$$v \sim \frac{1}{2} \sqrt{\frac{2 \times 800 \text{ V}}{m_{He}}} \sim 10^7 \text{ cm/sec} ,$$

implying a transit time of ~ 0.2 μsec . When the voltage is turned off, those ions with these velocities leave the discharge region and enter the acceleration region on this time scale. The rapid drop in cathode current just after voltage turn off is due to these fast ions.

The slow fall time phase can be understood with reference to Figure 21, which depicts the low-energy ions and electrons that were in the field-free negative glow region when the discharge circuit opened. These ions will enter the accelerating region under the influence of an ambipolar field. If the transmission of the accelerating grid were 100%,

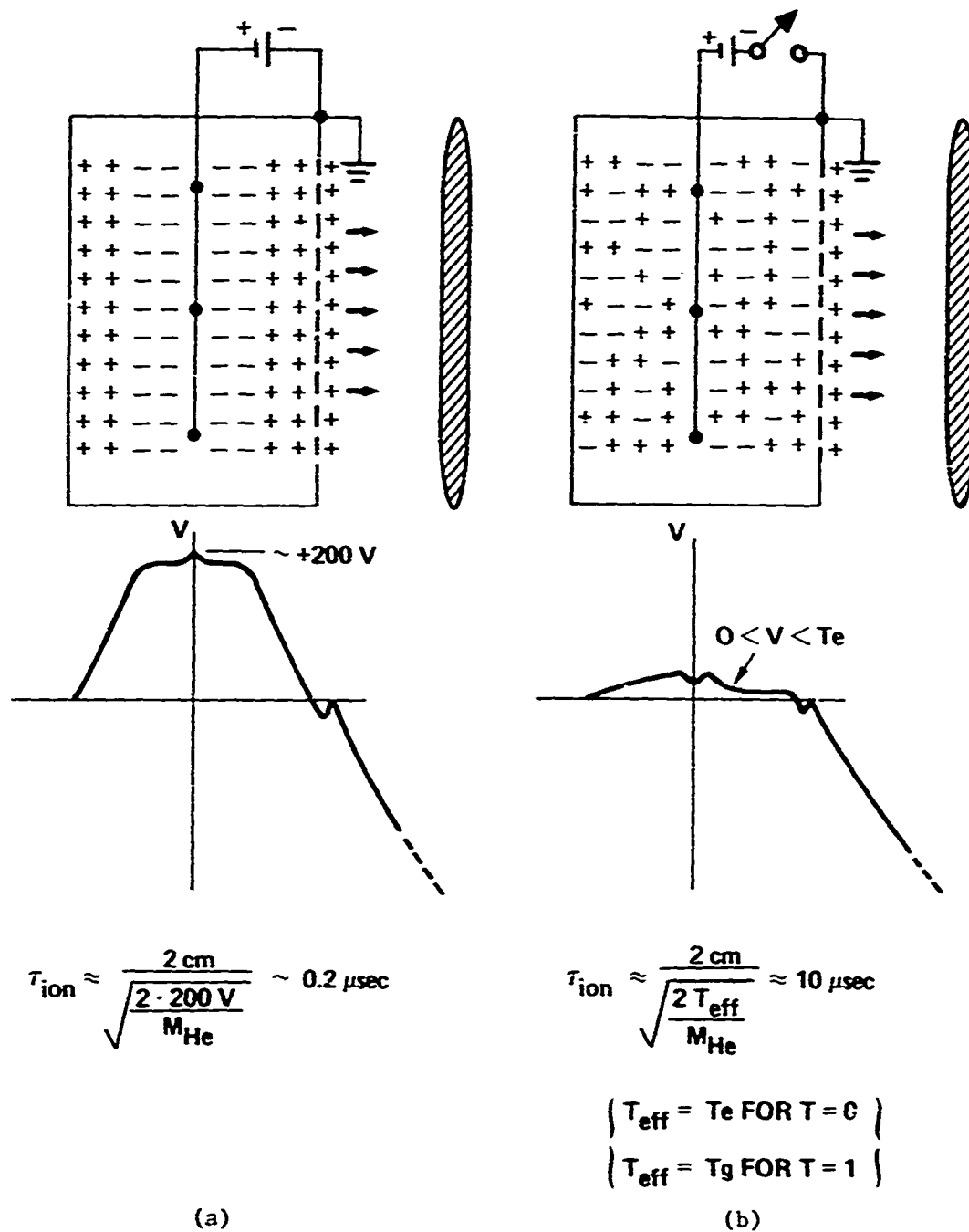


Figure 21. Particle and potential distribution in the discharge region.
(a) Voltage on. (b) Voltage off.

all electrons would be turned back by the accelerating field, the effective ambipolar field would be zero, and the ion's effective thermal drift would be given by the ion temperature, T_g (near room temperature). Because the walls of the wire discharge are grounded, the electrons can quickly dissipate the excess space charge flowing to ground. In the other extreme, if the transparency were zero, all electrons could escape by colliding with the "screen" and an ambipolar field would be present to retard the flow of electrons, giving rise to an ion temperature close to the electron temperature (~ 5 eV). The 80% transparent grid used will result in an effective ion temperature intermediate between these two extremes, but closer to room temperature than to the electron temperature. An order of magnitude estimate gives an effective transient time for the low-energy ions of ~ 10 μ sec, which is consistent with observation.

The long fall time of the beam current can be eliminated by eliminating the escape of low-energy ions from the wire discharge region. This can be accomplished in two ways. An auxiliary grid biased positive by only a few volts could be used on the low-voltage side of the accelerating grid to repel the ions. Alternatively, the wire discharge confining walls could be floated off ground, in which case the electron space charge would prevent the escape of ions.

SECTION 4

SUMMARY

Experiments were run and a comprehensive theoretical model developed that enabled the ion plasma e-gun to be more completely characterized. The experiments provided important high current data on the operation of the gun and of the thin-wire discharges. The theoretical model included consideration of 15 different reactions between helium atoms and ions and electrons and calculated the particle fluxes and the electric potential as a function of position in the high-voltage region. These calculated quantities accurately described the behavior of the gun at a beam voltage of 110 kV and enable projecting the operation of the e-gun at higher voltages (such as 400 keV) where the gun will be useful for pumping excimer lasers. A qualitative understanding was obtained of the transient behavior of both the e-gun and of the scaling properties of the thin-wire discharges.

The predicted scaled-up operation of the ion plasma e-gun for a 4-cm accelerating gap is shown in Figures 18 and 19. The high-voltage constraint at low pressure for the gun with this gap is vacuum breakdown between the electrodes. Data from different published reports on vacuum breakdown between planar and/or curved electrodes at field strengths near 100 kV/cm shows a great deal of variation. These results generally vary because of differences in the preparation of the electrode surfaces and the details of the vacuum pumping apparatus. Arc-free field strengths of 130 kV/cm were observed when there was careful attention to the details of preparing surfaces, etc., and field values of 90 kV/cm may be routinely obtained without breakdown. As a result, the operation of a 400-kV gun with a 4-cm gap seems technologically feasible. With these gun parameters, an electron current density of 9 A/cm^2 at a pressure of 20 mTorr of helium can be predicted (see Figure 18). At a higher gas pressure, say near 40 mTorr, the electron current density would be increased by $\approx 33\%$, implying 12 A/cm^2 at 400 kV with a 4-cm gap. With higher gas pressure, the high-voltage constraint is Paschen breakdown. Based on our previous results,⁸ the Paschen breakdown voltage at 40 mTorr and a 4-cm

gap is >480 kV. For a practical gun, outgassing of contaminants with a lower Paschen breakdown voltage would necessitate careful design of the gun to ensure maximum cleanliness and vacuum integrity. The use of flowing helium gas in the gun to maintain the proper pressure and to sweep out contaminants would be desirable. In conclusion, with proper attention to the technological details mentioned above, the operation of the ion plasma e-gun to obtain a 400 keV, 10 A/cm^2 (electron current) beam seems feasible.

Wire discharge studies indicate that the best results are obtained when (1) the wires are driven by a matched driving circuit such as a pulser-transformer combination, and (2) the thin-wire current is kept below 10 A. With the observed ion current densities on the present gun, this would require one wire every 1.2 to 1.5 cm along the long dimension of the gun. This wire spacing is quite practical.

In conclusion, we believe that the ion-plasma e-gun would be very useful for pumping repetitively pulsed e-beam and e-beam-sustained laser systems requiring a high-voltage (up to 400 kV), high-current-density beam (up to 10 A/cm^2). The gun has four compelling advantages:

- Monoenergetic e-beam: less foil heating, more uniform energy deposition in the laser gas.
- Long pulsewidth: 1 μsec to dc, larger average power for a given pulse-repetition frequency.
- Gun control with electronics at ground potential: no floating supplies, high voltage is not switched.
- Scalable.

A continuing program of development of the ion-plasma e-gun to demonstrate high-voltage operation and the pumping of a repetitively pulsed rare-gas monohalide excimer laser should be pursued.

REFERENCES

1. J.A. Mangano, J.H. Jacob, and J.B. Dodge, "Electron Beam-Controlled Discharge Pumping of the XeF Laser," Appl. Phys. Lett. 29, 426-428, 1 Oct. 1976.
2. L.F. Champagne, J.G. Eden, N.W. Harris, N. Djeu, and S.K. Searles, "1- μ s Laser Pulse from XeF," Appl. Phys. Lett. 30, 160-161, 1 Feb. 1977.
3. A.G. Hill, W.W. Beuchner, J.S. Clark, and J.B. Fisk, "The Emission of Secondary Electrons under High Energy Positive Ion Bombardment," Phys. Rev. 124, 969-982, 15 Nov. 1961.
4. G. Carter and J. Colligon, Ion Bombardment of Solids (London, Heineman, 1968), Ch. 3.
5. D. Pigache and G. Fournier, "Secondary Emission Electron Gun for High Pressure Molecular Lasers," J. Vac. Sci. Technol. 12, 1197-1199, Nov.-Dec. 1975.
6. W. Lotz, "An Empirical Formula for the Electron-Impact Ionization Cross Section," Z. Physik 206, 250-251 (1967).
7. G.W. McClure, "Low Pressure Glow Discharge," Appl. Phys. Lett. 2, 233-234, June 1963.
8. W.M. Clark, Jr. and G.J. Dunning, "A Long Pulse, High-Current Electron Gun for E-Beam Sustained Excimer Lasers," to be published in J. Quantum Electron. QE-14, Feb. 1978, and William Clark, "Electron Gun Technology," Final Report, contract N00014-72-C-0496, Hughes Research Laboratories, Malibu, CA, Dec. 1976.
9. G.W. McClure and K.D. Granzow, "High-Voltage Glow Discharges in D₂ Gas II Cathode Fall Theory," Phys. Rev. 125, 3-10, 1 Jan. 1962.
10. R.H. Hooverman, "Charged Particle Orbits in a Logarithm Potential," J. Appl. Phys. 34, 3505-3508, Dec. 1963.
11. A von Engel, Ionized Gases (Oxford Press, 1965), p. 227.
12. S.K. Allison, Rev. Mod. Phys. 30, 1137-1168, Oct. 1958.
13. S.W. Nagy, W.J. Savloa, Jr., and E. Poylack, Phys. Rev. 177, 71-76, 5 Jan. 1969.
14. J.B. Hasted, Atomic and Molecular Processes, D.R. Bates, Ed., (Academic, 1962), pp. 696-720.
15. K.H. Berkner, R.V. Pyle, J.W. Stearns, and J.C. Warren, "Single and Double-Electron Capture by 7.2 to 181 keV ³He⁺⁺ Ions in He," Phys. Rev. 166, 44-46, 5 Feb. 1968.

16. G.R. Hertel and W.S. Koski, "Cross Sections for the Single Charge Transfer of Doubly Charged Rare Gas Ions in Their Own Gases," J. Chem. Phys. 40, 3452-3453 (1964).
17. L.I. Pivovarov, M.T. Novikov, and V.M. Tubaev, "Electron Capture by Helium Ions in Various Gases in the 300-1500 keV Energy Range," Sov. Phys. JETP 15, 1035-1037, Dec. 1962.
18. L.J. Puckett, G.O. Taylor, and D.W. Martin, "Cross Sections for Ion and Electron Production in Gases by 0.15-1.00 meV Hydrogen and Helium Ions and Atoms," Phys. Rev. 178, 271-287, 5 Feb. 1969.
19. R.A. Langley, D.W. Martin, D.S. Harmer, J.W. Hooper, and E.W. McDaniel, "Cross Sections for Ion and Electron Production in Gases by Fast Helium (0.133 - 1.0 meV): I, Experimental," Phys. Rev. 136, A379-385, 19 Oct. 1964.
20. W. Lotz, "Electron-Impact Ionization Cross Sections and Ionization Rate Coefficient for Atoms and Ions," Astrophys. J. Suppl. Ser. XIV, No. 128, 207-237, May 1967.
21. L.J. Kieffer and G.H. Dunn, "Electron Impact Ionization Cross Section Data for Atoms, Atomic Ions, and Diatomic Molecules: I. Experimental Data," Rev. Mod. Phys. 38, 1-35, Jan. 1966.
22. M.J. Van Der Wiel, F.J. DeHeer, and G. Wiebes, "Double Ionization of Helium," Phys. Lett. 24A, 423-424, 10 Apr. 1967.
23. M.J. Van Der Wiel, Th.M. El-Sherbini, and L. Vriens, "Multiple Ionization of He, Ne, and Ar by 2-16 keV Electrons," Physica 42, 411-420 (1969).